

# Conductive Polymer Work Function Changes due to Residual Water: Impact of Temperature-Dependent Dielectric Constant

Ahmed E. Mansour, Hongwon Kim, Soohyung Park, Thorsten Schultz, David Xi Cao, Thuc-Quyen Nguyen, Wolfgang Brütting, Andreas Opitz, and Norbert Koch\*

Solution-processed conducting polymer thin films are key components in organic and flexible electronic and optoelectronic devices. An archetypal conducting polymer is poly(3,4-ethylenedioxythiophene)-poly(styrenesulfonate) (PEDOT:PSS), which can feature a high work function and thus helps achieving Ohmic contacts for holes with many semiconductors. However, it is known that residual water in PEDOT:PSS films lowers their work function and is detrimental for device lifetime. Our photoelectron spectroscopy experiments reveal that the work function of PEDOT:PSS films containing residual water shows the same trend as function of temperature as does the dielectric constant ( $\epsilon$ ) of water, in the range between 25 °C and –100 °C. Consistently, it is found from impedance spectroscopy measurements that  $\epsilon$  of residual water containing PEDOT:PSS films increases with decreasing temperature. After removal of residual water from PEDOT:PSS films by annealing in ultrahigh vacuum, the work function of thin films is much higher than before (reaching 6.1 eV) and, notably, independent of temperature. In contrast, no indication is found that the presence of residual water has any impact on the electrical conductivity. For a nominally water-free molecularly doped conjugated donor/acceptor copolymer films, a correlation between sample work function and temperature similar to those seen for PEDOT:PSS is found.

transistors.<sup>[1–4]</sup> Tremendous progress has been made in improving the performance and functionality of organic electronic devices. To a significant extent, this was possible by tuning the optical properties, electronic energy levels, and, foremost, charge transport properties of conductive polymers, as these are mostly employed as electrical contact layers. It should be noted that most polymers used in this field are semiconductors, and become sufficiently conductive only upon doping. Among the wide range of available polymers, polythiophenes have attracted attention for their moderate conductivity, high transparency, and air stability, which has enabled their implementation in various electronic and optoelectronic devices.<sup>[5–7]</sup> Molecular doping of polythiophenes, in which a small amount of dopant is added to the host polymer, has proven to be a successful approach to increase the density of mobile charge carriers and thus conductivity above 1 S cm<sup>-1</sup>.<sup>[8–14]</sup> A key challenge to the successful application of molecularly doped polymers lies in their relatively poor thermal stability, which ultimately leads to dopant diffusion and desorption at elevated temperatures.<sup>[15–17]</sup>

A conductive polymer from the thiophene family that presently dominates in device applications is p-doped poly(ethylenedioxythiophene) (PEDOT). The breakthrough of


## 1. Introduction

The discovery of conductive polymers has led to the development of flexible and low-cost solution-processed organic electronic devices, such as solar cells, light-emitting diodes, and field-effect

Dr. A. E. Mansour, Dr. S. Park, Dr. T. Schultz, Dr. A. Opitz, Prof. N. Koch  
Institut für Physik and IRIS Adlershof, Humboldt-Universität zu Berlin  
Berlin 12489, Germany

E-mail: norbert.koch@physik.hu-berlin.de

Dr. A. E. Mansour, Dr. S. Park, Dr. T. Schultz, Prof. N. Koch  
Helmholtz-Zentrum Berlin für Materialien und Energie GmbH  
Berlin 12489, Germany

 The ORCID identification number(s) for the author(s) of this article can be found under <https://doi.org/10.1002/aelm.202000408>.

© 2020 The Authors. Published by Wiley-VCH GmbH. This is an open access article under the terms of the Creative Commons Attribution License, which permits use, distribution and reproduction in any medium, provided the original work is properly cited.

H. Kim, Prof. W. Brütting  
Institute of Physics, University of Augsburg  
Augsburg 86159, Germany

Dr. S. Park  
Advanced Analysis Center  
Korea Institute of Science and Technology (KIST)  
Seoul 02792, South Korea

Dr. D. X. Cao, Prof. T.-Q. Nguyen  
Center for Polymers and Organic Solids  
Department of Chemistry and Biochemistry  
University of California  
Santa Barbara, CA 93106, USA

DOI: 10.1002/aelm.202000408

solution-processable PEDOT was achieved through combination with the water-soluble poly(styrenesulfonate) (PSS), where the polyanion PSS<sup>-</sup> acts as the counterion for the positive charges on PEDOT.<sup>[18]</sup> PEDOT:PSS is a water-soluble polyelectrolyte complex that exhibits a stable high conductivity, and thus has been widely used in research and industry.<sup>[19]</sup> Doped PEDOT is now available in numerous commercial formulations, with properties being varied via tuning the PEDOT:PSS ratio, solvent additives, and chemical structure of the counterion.<sup>[6]</sup> Due to the hydrophilic nature of PSS, thin films of PEDOT:PSS readily absorb water from the surrounding environment, with several percent water uptake at normal air humidity levels.<sup>[20,21]</sup> The presence of water in PEDOT:PSS thin films can have adverse effects on device stability and reproducibility. For example, degradation in organic solar cells was reported to accelerate by the presence of PEDOT:PSS due to increased water diffusion through the device, leading to delamination of the metal electrodes,<sup>[22]</sup> or deterioration of other organic components.<sup>[23]</sup> In addition, water-driven etching of indium tin oxide (ITO) at the interface with PEDOT:PSS negatively impact the device lifetime,<sup>[24]</sup> and minute amounts of water, even in a vacuum vessel, have been identified as one of the “killers” during fabrication of organic light-emitting diodes.<sup>[25]</sup>

PEDOT:PSS is commonly used as a hole transport layer in organic optoelectronics because of its comparably high work function. Accordingly, precise knowledge of the work function is crucial to predict the energy level alignment at interfaces, which determines device performance.<sup>[26,27]</sup> However, apparent variations of reported work function values of similar formulations of PEDOT:PSS are found in literature.<sup>[28–32]</sup> Despite the fact that annealing of as-prepared films of PEDOT:PSS in air at typically 150 °C has been established as standard procedure, such inconsistency has been ascribed to the inevitable presence of residual water in PEDOT:PSS films produced by different groups and lab environments. The difficulty to control amount of residual water is due to its ineffective removal from PEDOT:PSS films and possible reabsorption of water from the environment during device fabrication and operation.<sup>[33,34]</sup> Accordingly, carrying out the annealing step under different controlled environments (air, N<sub>2</sub>, O<sub>2</sub>) was shown to result in work function variations in the range of ≈200 meV.<sup>[35]</sup> The intrinsic work function of PEDOT:PSS was shown to be achievable only after removal of residual water; for an exemplary PEDOT:PSS formulation, the work function after annealing in air at 200 °C was 5.2 eV, but it increased to 5.65 eV after annealing in ultrahigh vacuum at ≈220 °C, and it returned to below 5.3 eV after even minute water vapor exposure.<sup>[33]</sup> This was attributed to both compositional changes<sup>[33,35]</sup> and water-aided dielectric screening of the local electric dipoles between the positively charged PEDOT and PSS anions.<sup>[33,36]</sup> These earlier studies on the effect of residual water on the work function of PEDOT:PSS have focused on the effect of residual water at room temperature and its removal upon annealing. This is in line with the conventional stability studies of organic electronic devices, in which the device performance is monitored at room temperature or at elevated temperatures. However, an extension of knowledge about the behavior of PEDOT:PSS to below room temperature appears desirable. For instance, valuable insights into the charge injection mechanism at electrode/semiconductor interfaces can be obtained from temperature-dependent current–voltage measurements extended below room

temperature,<sup>[37–40]</sup> and information about the photovoltaic gap in heterojunction solar cells can be extracted from a linear extrapolation of the temperature dependence of the open circuit voltage to 0 K.<sup>[40–42]</sup> Considering the influence of the high static dielectric constant  $\epsilon$  of water ( $\epsilon \approx 78$ )<sup>[43]</sup> and the influence of small amounts of residual water on the work function of PEDOT:PSS as discussed previously, it is thus important to extend studies toward low temperatures where the state of water could undergo a phase change and form ice or small clusters thereof. Notably, the dielectric constant of water increases with lower temperature and this trend continues for ice, i.e.,  $\epsilon$  increases from ≈90 at 0 °C to ≈170 at –150 °C.<sup>[43,44]</sup>

Beyond PEDOT:PSS, water could also play a role in other conductive polymers. The presence of water was shown to play a key role in the doping mechanism of the Lewis acid tris(pentafluorophenyl)borane [B(C<sub>6</sub>F<sub>5</sub>)<sub>3</sub>, BCF] mixed with conjugated polymers, such as poly(3-hexylthiophene) (P3HT). It was already shown earlier that water and BCF can form the monoadduct H<sub>2</sub>O·B(C<sub>6</sub>F<sub>5</sub>)<sub>3</sub>, which acts as H<sup>+</sup> source for protonation.<sup>[45]</sup> Such an adduct then protonates a polymer chain segment, which subsequently undergoes a charge transfer with a neighboring neutral segment resulting in p-doping.<sup>[46]</sup> Since the [HOB(C<sub>6</sub>F<sub>5</sub>)<sub>3</sub>]<sup>-</sup> anion is capable of forming hydrogen bonds,<sup>[45]</sup> additional water may be present in such doped polymer films, unless processing formally excludes the presence of water. Therefore, for such conductive polymers the eventual effect of residual water should also be an interesting subject of study.

In this work, we investigate the impact of residual water on the work function of different PEDOT:PSS formulations, including a nominally water-free one, as well as of BCF-doped P3HT down to –100 °C. We find that water in the conductive polymer films leads to a notable decrease of the work function upon cooling, while at the same time  $\epsilon$  increases. Once water is removed by annealing, the work function of the polymers is temperature independent. Remarkably, we find that the conductivity of PEDOT:PSS formulations is not affected by the presence of water. Finally, we demonstrate lowering of the hole injection barrier at interfaces between PEDOT:PSS and molecular semiconductor films upon water removal from the conducting polymers.

## 2. Results

We investigated two classes of conductive polymer systems: i) PEDOT of different formulations, namely, AI4083, HIL1.3, and HTL Solar 3, and ii) molecularly doped polymers with typically employed higher-end dopant molecules (D) to polymer monomer units (M) D:M ratio, namely, 7,7,8,8-tetracyano-2,3,5,6-tetrafluoroquinodimethane (F4TCNQ):P3HT (1:10),<sup>[9]</sup> F4TCNQ:poly[2,6-(4,4-bis[2-ethylhexyl]-4H-cyclopenta[2,1-*b*;3,4-*b'*)dithiophene)-*alt*-4,7(2,1,3-benzothiadiazole)] (PCPDTBT) (1:5),<sup>[47]</sup> and BCF:PCPDTBT (1:5).<sup>[46]</sup> The chemical structures of all compounds are shown in **Figure 1a**.

First, we discuss the sample work function as function of processing and temperature sequence. The work function was measured at temperatures ranging between –100 and +100 °C, following the sequence of steps during cooling/heating cycles in UHV, as indicated. The work function of as-prepared thin films was first measured at room temperature (RT\*), within

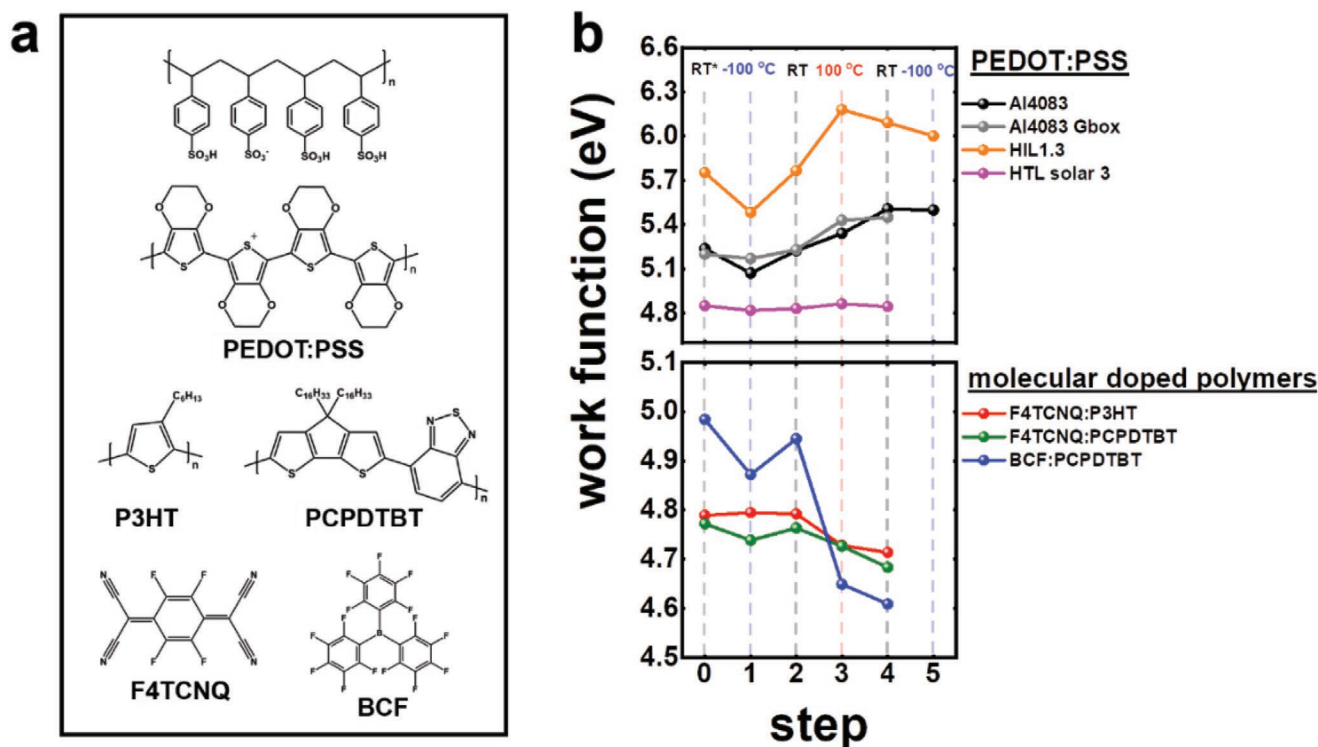


**Figure 1.** a) The chemical structure of compounds used in this work. b) Work function of different conductive polymers measured by UPS at each temperature step of the cooling/heating cycles as detailed in the text. The vertical dashed lines label the temperature at which the work function was determined.

1 h of introducing the sample to the UHV system (step 0) to minimize eventual water desorption from the samples. This is followed by cooling to  $-100\text{ °C}$  (step 1). Then, the sample is warmed up back to room temperature (step 2). After that, annealing at  $+100\text{ °C}$  (step 3) follows, cooling down to room temperature (step 4), and for selected samples another measurement at  $-100\text{ °C}$  (step 5). The work function was measured at each step (0→5) at the respective temperature. As benchmark to assess the effect of water desorption from the films in UHV at RT on the measured work function, a HIL1.3 sample was measured at RT after 1 h and after 20 h residing in UHV. The resulting work function change was less than 50 meV.

As shown in the top panel of Figure 1b, the work function of AI4083 and HIL1.3 changes with temperature except for the water-free HTL Solar 3, which remains constant at  $\approx 4.80\text{ eV}$ . Upon cooling to  $-100\text{ °C}$  (step 1), the work function decreases for AI4083 (from 5.25 to 5.05 eV) and for HIL1.3 (from 5.75 to 5.48 eV). The initial work function values are recovered once the samples are brought back to RT (step 2). Upon heating to  $100\text{ °C}$  (step 3) the work function increases to 5.35 eV (AI4083) and 6.20 eV (HIL1.3). This increase in work function is mostly irreversible, since back at RT (step 4) and further cooled down to  $-100\text{ °C}$  (step 5) there are only small further changes. A similar step-dependence was observed for the sample AI4083 Gbox [initial annealing in the glove box with low water content ( $<0.1\text{ ppm}$ ) and transferred to UHV without air exposure].

The work function of PEDOT:PSS originates from contributions of the bulk chemical potential of electrons, which determines the energy of the Fermi level, and surface dipoles ( $\mu_{\perp}$ ) pointing from  $\text{PSS}^{-}$  to  $\text{PEDOT}^{+}$ , which contributes to the vacuum

level position with respect to the Fermi level. The latter contribution to the work function ( $\Phi_{\text{SD}}$ ) is due to the PSS-rich surface of PEDOT:PSS films,<sup>[48,49]</sup> and thus a preferential orientation of the local anion–cation dipoles  $\mu$ , giving the net dipole component perpendicular to the surface  $\mu_{\perp}$ . According to the Helmholtz equation  $\Phi_{\text{SD}}$ , being dependent on  $\epsilon$ , can be calculated as<sup>[50]</sup>

$$\Phi_{\text{SD}} = \frac{qN\mu_{\perp}}{\epsilon_0\epsilon} \quad (1)$$

where  $q$  is the elementary charge,  $N$  the density of surface dipoles,  $\epsilon$  the dielectric constant, and  $\epsilon_0$  the vacuum permittivity. At room temperature, as-prepared PEDOT:PSS films contain residual water, unless annealed in UHV, as discussed previously.<sup>[20,21,33]</sup> Water has a high dielectric constant of  $\approx 78$  at room temperature,<sup>[43]</sup> and thus its presence in PEDOT:PSS could increase the dielectric constant of the film, even if the water molecules are bound to the ions of the polymer and not in pure liquid phase. An increased  $\epsilon$  leads to a lowering of  $\Phi_{\text{SD}}$  according to Equation (1), and thus of the sample work function, compared to a film without any residual water. With this, we can readily understand the (irreversible) work function increase of AI4083 and HIL1.3 upon heating (step 3), as residual water leaves the samples,  $\epsilon$  becomes lower, and  $\Phi_{\text{SD}}$  and the work function increase. Notably, even when the annealing step during film preparation is carried out in the low water content atmosphere of the glovebox (sample AI4083 Gbox), standard PEDOT:PSS is sufficiently hygroscopic to absorb water, as also for this sample step 3 significantly increases the work function. The constant work function of HTL Solar 3, on the other hand, thus indicates

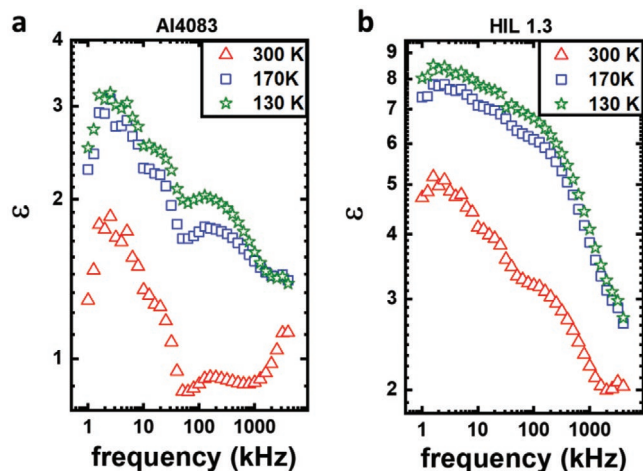


**Figure 2.** a,b) The dielectric constant  $\epsilon$  of residual water-containing AI4083 and HIL1.3 thin films as function of frequency for different temperatures. For both water-containing polymer films,  $\epsilon$  increases for decreasing temperature. The decrease of  $\epsilon$  below a frequency of about 2 kHz is an artifact of the measurement system caused by the finite phase resolution of the instrument.

that it is indeed water-free, or at least the amount of residual water is sufficiently low to not impact the work function.

We now turn to the work function at  $-100\text{ }^{\circ}\text{C}$  (step 1), where it can be expected that residual water in the samples freezes, forming small ice clusters, as suggested earlier.<sup>[48]</sup> Since  $\epsilon$  of ice at this temperature is almost twice as large as the values of water at RT,<sup>[44]</sup> we can expect an according increase of the effective  $\epsilon$  of PEDOT:PSS films containing residual water. Note that  $\epsilon$  of different structures of ice has been extensively investigated both experimentally and theoretically and was found to be  $\approx 150$  at  $-100\text{ }^{\circ}\text{C}$  for disordered structures, which are relevant to the temperature and pressure ranges used in our work.<sup>[44,51]</sup> To validate our proposition, we determined the dielectric constant of AI4083 and HIL1.3 films from impedance measurements over a wide frequency range. As can be seen from the data in **Figure 2**,  $\epsilon$  of both residual water-containing polymer films increases significantly with decreasing temperature. The higher  $\epsilon$  of the films at  $-100\text{ }^{\circ}\text{C}$  as compared to RT leads to a stronger screening of the surface dipoles according to Equation (1) and thus significantly *decreases* the work function, as measured to be  $\approx 170\text{ meV}$  for AI4083 and  $\approx 270\text{ meV}$  for HIL1.3 (compared to RT). This interpretation is supported by the observation that after cooling (step 1) the work function values return to the initial ones at RT of step 2. Furthermore, once the samples were annealed at  $+100\text{ }^{\circ}\text{C}$  in UHV (step 3), i.e., most of the residual water removed from the films, no significant further changes in sample work function are observed, even when cooling to  $-100\text{ }^{\circ}\text{C}$  (see steps 4 and 5 in **Figure 1b**). The overall work function change is more pronounced for HIL1.3 than for AI4083, which points toward a stronger hygroscopic nature. We also observe that the work function of HIL1.3 decreases slightly from step 3 to steps 4 and 5. This is a sign for the presence of still some residual water, also after annealing to  $+100\text{ }^{\circ}\text{C}$  in UHV. This, however, is fully in line with the previous finding that full water removal in UHV proceeded only around  $+200\text{ }^{\circ}\text{C}$  for similar annealing durations.<sup>[33]</sup>

Next, we discuss the work function changes observed in molecularly doped P3HT and PCPDTBT, summarized in the bottom panel of **Figure 1b**. The measured work function at RT\* (step 0) of F4TCNQ:P3HT and F4TCNQ:PCPDTBT is  $\approx 4.80\text{ eV}$  and that of BCF:PCPDTBT is  $\approx 5.0\text{ eV}$ . Upon cooling the films to  $-100\text{ }^{\circ}\text{C}$  (step 1), the work function of PCPDTBT doped with either F4TCNQ or BCF decreases as compared to its value at RT\*; yet the decrease is more pronounced for BCF with a decrease of  $\approx 110\text{ meV}$ . Once back at RT (step 2), the work function values return to their original ones. In contrast, the work function of F4TCNQ:P3HT stays constant. Upon heating to  $+100\text{ }^{\circ}\text{C}$  (step 3), the work function decreases for all samples, which can readily be assigned to be due to thermal dopant desorption.<sup>[15,16]</sup> From this step on, further investigations of the influence of removing residual water from these samples are precluded. The observed decrease of the work function at  $-100\text{ }^{\circ}\text{C}$  for BCF:PCPDTBT and F4TCNQ:PCPDTBT films is analogous to the changes observed for PEDOT:PSS discussed previously. The changes for PCPDTBT might thus also be ascribed to the presence of water in the as-prepared samples at RT. At  $-100\text{ }^{\circ}\text{C}$ , residual water increases the effective  $\epsilon$  of the film and, in turn, decreases the work function. The reduction in work function at  $-100\text{ }^{\circ}\text{C}$  is more pronounced in BCF:PCPDTBT, which would be in line with the hygroscopic nature of BCF.<sup>[46]</sup> However, this interpretation would require that both BCF and F4TCNQ-doped PCPDTBT films have an enrichment of dopant anions at the surface, as only this would result in a notable  $\mu_{\perp}$  and thus a contribution of  $\Phi_{\text{SD}}$  to the overall work function, as discussed previously for PEDOT:PSS. However, the comparably low molecular weight, and thus high volatility, of BCF and F4TCNQ render this scenario unlikely. In fact, for F4TCNQ-doped PCPDTBT we find from angle-dependent X-ray photoelectron spectroscopy (XPS), monitoring the fluorine-to-sulfur ratio (see **Table 1**), that the film surface is actually slightly depleted of F4TCNQ compared to the bulk. Possibly, temperature-dependent conformational changes of the polymer could modify the frontier energy levels available for electron transfer to the dopants, or bulk effects related to doping occur upon a modified dielectric constant. On the other hand, the work function F4TCNQ:P3HT is independent of temperature below RT, which indicates negligible water presence or less influence of low temperature on the frontier energy levels available for doping.

To estimate the amount of residual water present in PEDOT:PSS (AI4083) thin films, we compared the atomic ratio of oxygen to sulfur (O/S) in the as-prepared film to that after annealing at  $+100\text{ }^{\circ}\text{C}$ . The atomic ratio was calculated from O 1s and S 2p spectra measured by XPS. The O/S in the as-prepared thin film (step 0) was  $\approx 2.7$ , and decreased after annealing

**Table 1.** The fluorine-to-sulfur atomic ratio (F/S) for a F4:PCPDTBT (1:5) thin film as function of electron take-off angle ( $90^{\circ}$  corresponds to surface-normal emission) from angle-dependent XPS.

Electron take-off angle [ $^{\circ}$ ]	F/S
90	0.18
70	0.15
40	0.12



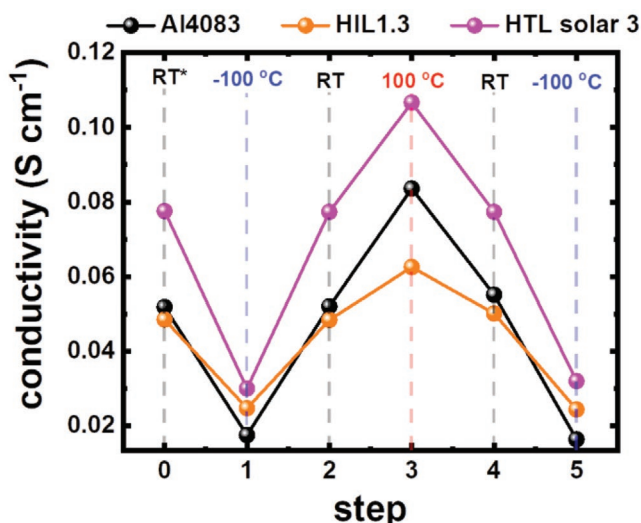


**Figure 3.** Conductivity of PEDOT:PSS Al4083, HIL1.3, and PEDOT:complex HTL Solar 3 thin films at each temperature step during the cooling/heating cycles. The vertical dashed lines label the temperature at which the conductivity was measured.

(step 5) to  $\approx 2.4$ . The removal of residual water after annealing PEDOT:PSS reduces the amount of oxygen, which should indeed decrease O/S.<sup>[52]</sup> The amount of residual water was estimated assuming that the total change in the O/S value of 0.3 is due to loss of water from a homogeneous PEDOT:PSS thin film. Based on the unit cell volume of PEDOT:PSS (containing four monomer units) of  $2027 \text{ \AA}^3$ ,<sup>[53]</sup> and the fact that  $\text{H}_2\text{O}$  molecules form hydrogen bonds with PSS, the volume fraction of residual water is estimated to be  $\approx 1.7\%$ , corresponding to  $5.7 \times 10^{20} \text{ H}_2\text{O molecules cm}^{-3}$ , which agrees with previous reports.<sup>[21,48]</sup> This water density translates for our PEDOT:PSS film ( $1 \text{ cm}^2 \times 70 \text{ nm}$ ) into an uptake of  $1.20 \times 10^{-7} \text{ cm}^3$  of water, which is indeed readily available in a standard glove box ( $0.1 \text{ ppm H}_2\text{O}$  and  $1 \text{ m}^3$  box volume correspond to a water volume of  $\approx 7 \times 10^{-5} \text{ cm}^3$ ).

Having elucidated the fundamental impact of residual water on the work function of conductive polymers films, we next attend to its influence on the electrical conductivity. Figure 3 shows the changes in the electrical conductivity of Al4083, HIL1.3, and HTL Solar 3 films. For all three materials, the conductivity at  $-100 \text{ }^\circ\text{C}$  is lower than at RT, and higher at  $+100 \text{ }^\circ\text{C}$ . This behavior of conductivity with temperature is expected, as it is characteristic of the typical hopping transport in disordered semiconductors, such as PEDOT:PSS.<sup>[48,54,55]</sup> Notably, for all three formulations, the conductivity changes are fully reversible. We evaluated the activation energy of charge transport for the films before (steps 1 and 2) and after (steps 3, 4, and 5) removing residual water. The activation energy shows a negligible change once water is removed from the film within the uncertainty of our measurements. The activation energy values change for Al4083 from 38 to 45 meV, for HIL1.3 changes from 24 to 26 meV, and for HTL Solar 3 it stays at 33 meV. This indicates that residual water and its physical state in the bulk of the polymer has no apparent influence on the electrical conductivity of PEDOT:PSS films.

Finally, we exemplarily investigate the effect of the presence of water in PEDOT:PSS (Al4083 and HIL1.3) thin films on the interfacial energy levels with 5 nm thick films of the molecular semiconductor 2,2',7,7'-tetrakis(carbazol-9-yl)-9,9-spirobifluorene (s-CBP). The ionization energy of s-CBP was determined from our ultraviolet photoelectron spectroscopy (UPS) measurements to be 6.10 eV. Accordingly, it is expected that increasing the work function of the PEDOT:PSS substrate by removing residual water (Figure 1b) should result in a reduction of the hole injection barrier at the interface, as long as Fermi level pinning has not set in.<sup>[56,57]</sup> Specifically, two cases are compared: i) depositing s-CBP on as-prepared PEDOT:PSS (containing residual water), followed by annealing at  $+100 \text{ }^\circ\text{C}$  in UHV (dep./ann.), and ii) annealing PEDOT:PSS at  $+100 \text{ }^\circ\text{C}$  in UHV to remove most of the residual water, and then depositing s-CBP at RT (ann./dep.). UPS measurements were carried out at RT to obtain the sample work function and the binding energy of the highest occupied molecular orbital (HOMO) level with respect to the Fermi level, the latter directly corresponding to the hole injection barrier at the interface. The results are summarized in the scheme of Figure 4. For the Al4083/s-CBP interface (top panel of Figure 4), vacuum level alignment prevails throughout, i.e., Fermi level pinning has not set in and the molecular energy levels are expected to move in parallel with the substrate work function. In the case of the dep./ann. sequence, the reduction of the hole injection barrier is negligible ( $\approx 50 \text{ meV}$ ). This is unexpected, as we observed a significant increase of the bare polymer work function upon annealing and concomitant water removal (up to 5.4 eV, see Figure 1b),

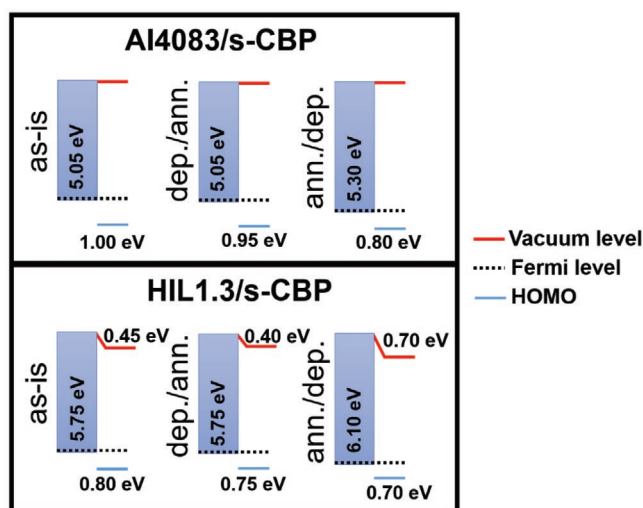


**Figure 4.** Influence of annealing on the energy level alignment between PEDOT:PSS and s-CBP (5 nm) for Al4083 (top panel) and HIL1.3 (bottom panel). Three cases are shown for each: i) as-deposited s-CBP on as-prepared PEDOT:PSS without annealing (as-is), ii) s-CBP on as-prepared PEDOT:PSS followed by annealing ( $+100 \text{ }^\circ\text{C}$ ) (dep./ann.), and iii) s-CBP on PEDOT:PSS annealed ( $+100 \text{ }^\circ\text{C}$ ) prior to molecular layer deposition (ann./dep.). The Fermi level is shown as dashed black line, the vacuum level after s-CBP deposition is indicated with the red line and the value of the work function change. The onset of the highest occupied molecular orbital (HOMO) level is the blue solid line, with the value of the hole injection barrier.

which should reduce the hole injection barrier accordingly. From the present observation, we thus conclude that the desorption of water from PEDOT:PSS is substantially slowed down by the presence of the s-CBP layer on top. In contrast, the ann./dep. sequence assures the effective removal of residual water and increase of the work function prior to the deposition of s-CBP. Consequently, a decrease in the hole injection barrier at the interface by  $\approx 150$  meV compared to the pristine interface is observed. In the case of the HIL1.3/s-CBP interfaces (bottom panel of Figure 4), Fermi level pinning prevails throughout (indicated by the work function reduction upon s-CBP deposition), as the work function of this PEDOT:PSS formulation is very high (5.75 eV) already with residual water. Accordingly, the hole injection barrier exhibits a negligible change in either case of dep./ann. or ann./dep. sequences. Thus, the hole injection barrier at the interface of high ionization energy organic semiconductors with PEDOT:PSS can be minimized if the latter is annealed in UHV prior to deposition or the semiconductor, to assure an effective removal of residual water and high work function.

### 3. Conclusion

It had been suggested earlier that residual water in PEDOT:PSS films lowers the work function due to dielectric screening of the thin films' surface dipole (between subsurface PEDOT<sup>+</sup> and surface PSS<sup>-</sup>). Here, we substantiate this model by demonstrating that the work function of as-prepared PEDOT:PSS changes reversibly between room temperature and  $-100$  °C, with lower work function values at lower temperature. This is in line with the almost twofold increase of the dielectric constant of residual water-containing PEDOT:PSS films when going from RT to  $-140$  °C. We acknowledge that the form of water inside PEDOT:PSS films differs from its pure solid and liquid form, but the correlation between work function and  $\epsilon$  of water is striking. Additionally, after removal of residual water from PEDOT:PSS by annealing in UHV, the work function is significantly increased and, notably, no longer temperature dependent, between  $-100$  and  $+100$  °C. For films made from a water-free formulation of PEDOT (HTL Solar 3) the work function is always independent of temperature. These observations further support our model. In contrast, we find no evidence for an influence of residual water in the bulk of PEDOT:PSS films on charge transport. From an electronic device perspective, minimizing the hole injection barrier at interfaces between PEDOT:PSS and organic semiconductors, i.e., achieving the highest possible electrode work function, necessitates water removal from PEDOT:PSS before deposition of the semiconductor layer. We find indications that annealing-induced water desorption from PEDOT:PSS is substantially slowed down already by a 5 nm thick s-CBP layer.

Remarkably, for molecularly doped films of the semiconductor polymer PCPDTBT, we find the same correlation between work function and temperature (at and below RT) as for PEDOT:PSS. While it appears plausible that the dopant BCF introduces some water in the samples, this is more questionable for the F4TCNQ dopant. However, the existence

of surface dipoles, prerequisite for the applicability of our model developed for PEDOT:PSS, has not been demonstrated yet for molecularly doped polymers. Furthermore, F4TCNQ-doped P3HT films show no temperature-dependent work function (at and below RT). Future efforts should thus be directed toward elucidating the mechanisms behind a temperature dependence of the work function of doped polymer thin films.

### 4. Experimental Section

**Materials and Sample Fabrication:** Aqueous dispersions of PEDOT:PSS AI4083 and of PEDOT:PSS HIL1.3 were obtained from Ossila (Product No. M121) and H.C. Starck GmbH, respectively. Water-free PEDOT:complex HTL Solar 3 in toluene was obtained from Ossila (Product No. M125). All solutions were filtered using nylon filters (450 nm pore size) prior to thin film preparation. Thin films were prepared by spin-coating on solvent-cleaned and UV-ozone-treated ITO on glass substrates. AI4083 and HIL1.3 films ( $\approx 50$  nm) were prepared in air, using a spin speed of 3000 rpm for 100 s, followed by annealing in air at  $150$  °C for 15 min. One sample of AI4083 (AI4083 Gbox) was spin-coated in air but the annealing step was carried out in nitrogen-filled glovebox ( $O_2$  and  $H_2O < 0.1$  ppm). HTL Solar 3 films ( $\approx 70$  nm) were prepared in the glovebox at a spin speed of 5000 rpm for 100 s, followed by annealing in the glovebox at  $150$  °C for 15 min. AI4083 Gbox and HTL Solar 3 samples were transferred for subsequent characterization without exposure to the ambient.

P3HT ( $M_w = 60.2$  kg mol<sup>-1</sup>, regioregularity of 97.6%) was purchased from Merck KGaA (Product No. Lisicon SP001). PCPDTBT was obtained from 1-Material Inc. Both polymers were used as received. The molecular dopants BCF (Product No. T2313) and F4TCNQ (Product No. T1131) were obtained from TCI Deutschland GmbH. Doped polymers were prepared by solution mixing in the glovebox. Anhydrous chloroform (Sigma-Aldrich) was used as solvent. Different volumes were used to set the mixing ratio, which is given as the ratio of dopant molecules (D) to polymer monomer units (M), i.e., D:M. Thin films of molecularly doped polymers were prepared by spin-coating (2000 rpm) in the glovebox without any subsequent annealing and were transferred without exposure to the ambient for subsequent characterization.

s-CBP was purchased from Lumtec Corp. (Product No. LT-N416) and used as received. Thin films of s-CBP ( $\approx 5$  nm) were deposited in ultrahigh vacuum (UHV) by thermal evaporation.

**Characterization:** UPS and XPS were conducted in a custom multichamber UHV system ( $\approx 5 \times 10^{-10}$  mbar) using a hemispherical electron analyzer (Scienta DA30L) with 105 meV energy resolution, and excitation with Mg K $\alpha$  (1253.6 eV, XPS) and He I (21.22 eV, UPS), in UHV of  $\approx 5 \times 10^{-10}$  mbar. To avoid sample damage by ultraviolet radiation, the He discharge lamp was operated at a low discharge current of 30 mA to reduce the photon flux. In addition, radiation exposure time of the samples was minimized in the workflow. The sample work function was obtained from the secondary electron cutoff (SECO) measured at sample bias of  $-10$  V.

Thin films for electrical conductivity measurements were prepared on prepatterned ITO substrates purchased from Ossila (Product No. S162). The conductivity measurements were carried out with a Keithley 4200-SCS parameter analyzer in a high vacuum cryostat ( $\approx 4 \times 10^{-7}$  mbar) by recording the slopes of linear current-voltage characteristics in the voltage range  $-2.5$  to  $+2.5$  V and using an in-plane geometry.

Both photoemission and electrical measurements were performed at different temperatures [ $-100$  °C,  $25$  °C (RT),  $+100$  °C] in a well-defined sequence as detailed in the Results section.

The impedance and capacitance of AI4083 and HIL1.3 were measured using a Solartron 1260 Impedance analyzer in the frequency range between  $1$  and  $5 \times 10^6$  Hz. The voltage applied was 100 mV AC, in addition to a DC voltage ranging between  $-0.5$  and  $1.0$  V. Both AI4083

(125 nm) and HIL1.3 (195 nm) were spin-coated on ITO substrates, followed by evaporation of Ag (100 nm) as top electrode. The active area of these devices was 1 mm<sup>2</sup>. The measurements were performed in high vacuum (10<sup>-6</sup> mbar) between room temperature and 130 K.

## Acknowledgements

The authors acknowledge funding by the Deutsche Forschungsgemeinschaft (DFG) (Project Nos. 18208777-SFB 951, 239543752-BR1728/14-2, and 286798544-SA 2916/1-1). D.X.C. and T.-Q.N. acknowledge the support from the Department of Energy under Award no. DE-SC0017659. Open access funding enabled and organized by Projekt DEAL.

## Conflict of Interest

The authors declare no conflict of interest.

## Keywords

conductive polymers, dielectric constant, temperature dependence, water, work function

Received: April 20, 2020

Revised: July 21, 2020

Published online: September 11, 2020

- [1] T. K. Das, S. Prusty, *Polym.-Plast. Technol. Eng.* **2012**, *51*, 1487.
- [2] Y. Wang, C. Zhu, R. Pfattner, H. Yan, L. Jin, S. Chen, F. Molina-Lopez, F. Lissel, J. Liu, N. I. Rabiah, Z. Chen, J. W. Chung, C. Linder, M. F. Toney, B. Murmann, Z. Bao, *Sci. Adv.* **2017**, *3*, e1602076.
- [3] H. Yao, Z. Fan, P. Li, B. Li, X. Guan, D. Du, J. Ouyang, *J. Mater. Chem. A* **2018**, *6*, 24496.
- [4] M. Nikolka, K. Broch, J. Armitage, D. Hanifi, P. J. Nowack, D. Venkateshvaran, A. Sadhanala, J. Saska, M. Mascal, S. H. Jung, J. K. Lee, I. McCulloch, A. Salleo, H. Sirringhaus, *Nat. Commun.* **2019**, *10*, 2122.
- [5] U. Mehmood, A. Al-Ahmed, I. A. Hussein, *Renewable Sustainable Energy Rev.* **2016**, *57*, 550.
- [6] Y. Wen, J. Xu, *J. Polym. Sci., Part A: Polym. Chem.* **2017**, *55*, 1121.
- [7] R. D. McCullough, *Adv. Mater.* **1998**, *10*, 93.
- [8] E. F. Aziz, A. Vollmer, S. Eisebitt, W. Eberhardt, P. Pingel, D. Neher, N. Koch, *Adv. Mater.* **2007**, *19*, 3257.
- [9] P. Pingel, D. Neher, *Phys. Rev. B* **2013**, *87*, 115209.
- [10] D. T. Scholes, S. A. Hawks, P. Y. Yee, H. Wu, J. R. Lindemuth, S. H. Tolbert, B. J. Schwartz, *J. Phys. Chem. Lett.* **2015**, *6*, 4786.
- [11] Y. Karpov, T. Erdmann, M. Stamm, U. Lappan, O. Guskova, M. Malanin, I. Raguzin, T. Beryozkina, V. Bakulev, F. Günther, S. Gemming, G. Seifert, M. Hamsch, S. Mannsfeld, B. Voit, A. Kiri, *Macromolecules* **2017**, *50*, 914.
- [12] J. Hynynen, D. Kiefer, L. Yu, R. Kroon, R. Munir, A. Amassian, M. Kemerink, C. Müller, *Macromolecules* **2017**, *50*, 8140.
- [13] L. Chen, W. Liu, Y. Yan, X. Su, S. Xiao, X. Lu, C. Uher, X. Tang, *J. Mater. Chem. C* **2019**, *7*, 2333.
- [14] K. E. Watts, B. Neelamraju, E. L. Ratcliff, J. E. Pemberton, *Chem. Mater.* **2019**, *31*, 6986.
- [15] P. Reiser, L. Müller, V. Sivanesan, R. Lovrincic, S. Barlow, S. R. Marder, A. Pucci, W. Jaegermann, E. Mankel, S. Beck, *J. Phys. Chem. C* **2018**, *122*, 14518.
- [16] H. Hase, K. O'Neill, J. Frisch, A. Opitz, N. Koch, I. Salzmann, *J. Phys. Chem. C* **2018**, *122*, 25893.
- [17] J. Li, C. W. Rochester, I. E. Jacobs, E. W. Aasen, S. Friedrich, P. Stroeve, A. J. Moulé, *Org. Electron.* **2016**, *33*, 23.
- [18] A. Elschner, S. Kirchmeyer, W. Lövenich, U. Merker, K. Reuter, *PEDOT: Principles and Applications of an Intrinsically Conductive Polymer*, CRC Press, Boca Raton, FL **2010**.
- [19] L. Groenendaal, F. Jonas, D. Freitag, H. Pielartzik, J. R. Reynolds, *Adv. Mater.* **2000**, *12*, 481.
- [20] L. Zhanshayeva, V. Favaron, G. Lubineau, *ACS Omega* **2019**, *4*, 21883.
- [21] Q. Wei, M. Mukaida, W. Ding, T. Ishida, *RSC Adv.* **2018**, *8*, 12540.
- [22] T. S. Glen, N. W. Scarratt, H. Yi, A. Iraqi, T. Wang, J. Kingsley, A. R. Buckley, D. G. Lidzey, A. M. Donald, *J. Polym. Sci., Part B: Polym. Phys.* **2016**, *54*, 216.
- [23] M. Jørgensen, K. Norrman, F. C. Krebs, *Sol. Energy Mater. Sol. Cells* **2008**, *92*, 686.
- [24] M. P. De Jong, L. J. Van Ijzendoorn, M. J. A. De Voigt, *Appl. Phys. Lett.* **2000**, *77*, 2255.
- [25] H. Fujimoto, T. Nakamura, K. Nagayoshi, K. Harada, H. Miyazaki, T. Kurata, J. Kiyota, C. Adachi, *Appl. Phys. Lett.* **2020**, *116*, 143301.
- [26] H. Ishii, K. Sugiyama, E. Ito, K. Seki, *Adv. Mater.* **1999**, *11*, 605.
- [27] N. Koch, *ChemPhysChem* **2007**, *8*, 1438.
- [28] H. Peisert, A. Petr, L. Dunsch, T. Chassé, M. Knupfer, *ChemPhysChem* **2007**, *8*, 386.
- [29] A. Moujoud, S. H. Oh, H. S. Shin, H. J. Kim, *Phys. Status Solidi A* **2010**, *207*, 1704.
- [30] W. Jang, S. Ahn, S. Park, J. H. Park, D. H. Wang, *Nanoscale* **2016**, *8*, 19557.
- [31] W. Kim, N. Kim, J. K. Kim, I. Park, Y. S. Choi, D. H. Wang, H. Chae, J. H. Park, *ChemSusChem* **2013**, *6*, 1070.
- [32] Y. Zhang, L. Chen, X. Hu, L. Zhang, Y. Chen, *Sci. Rep.* **2015**, *5*, 12839.
- [33] N. Koch, A. Vollmer, A. Elschner, *Appl. Phys. Lett.* **2007**, *90*, 043512.
- [34] D.-J. Yun, H. Ra, J. Kim, I. Hwang, J. Lee, S.-W. Rhee, J. Chung, *ECS J. Solid State Sci. Technol.* **2012**, *1*, M10.
- [35] J. Huang, P. F. Miller, J. S. Wilson, A. J. de Mello, J. C. de Mello, D. D. C. Bradley, *Adv. Funct. Mater.* **2005**, *15*, 290.
- [36] E. S. Muckley, C. B. Jacobs, K. Vidal, J. P. Mahalik, R. Kumar, B. G. Sumpter, I. N. Ivanov, *ACS Appl. Mater. Interfaces* **2017**, *9*, 15880.
- [37] M. Koehler, I. A. Hümmelgen, *Appl. Phys. Lett.* **1997**, *70*, 3254.
- [38] H. Vestweber, J. Pommerehne, R. Sander, R. F. Mahrt, A. Greiner, W. Heitz, H. Bässler, *Synth. Met.* **1995**, *68*, 263.
- [39] M. Bär, T. Schnabel, J. H. Alsmeyer, S. Krause, N. Koch, R. G. Wilks, E. Ahlswede, *ACS Appl. Energy Mater.* **2018**, *1*, 475.
- [40] H. Li, D. He, Q. Zhou, P. Mao, J. Cao, L. Ding, J. Wang, *Sci. Rep.* **2017**, *7*, 40134.
- [41] K. Vandewal, K. Tvingstedt, A. Gadisa, O. Inganäs, J. V. Manca, *Phys. Rev. B* **2010**, *81*, 125204.
- [42] M. Gruber, J. Wagner, K. Klein, U. Hörmann, A. Opitz, M. Stutzmann, W. Brütting, *Adv. Energy Mater.* **2012**, *2*, 1100.
- [43] D. Bertolini, M. Cassettari, G. Salvetti, *J. Chem. Phys.* **1982**, *76*, 3285.
- [44] G. P. Johari, E. Whalley, *J. Chem. Phys.* **1981**, *75*, 1333.
- [45] L. H. Doerr, M. L. H. Green, *J. Chem. Soc., Dalton Trans.* **1999**, 4325.
- [46] B. Yurash, D. X. Cao, V. V. Brus, D. Leifert, M. Wang, A. Dixon, M. Seifrid, A. E. Mansour, D. Lungwitz, T. Liu, P. J. Santiago, K. R. Graham, N. Koch, G. C. Bazan, T.-Q. Q. Nguyen, *Nat. Mater.* **2019**, *18*, 1327.
- [47] M. Ivanović, H. Peisert, T. Chassé, *Org. Electron.* **2016**, *39*, 267.
- [48] J. Zhou, D. H. Anjum, L. Chen, X. Xu, I. A. Ventura, L. Jiang, G. Lubineau, *J. Mater. Chem. C* **2014**, *2*, 9903.
- [49] U. Lang, E. Müller, N. Naujoks, J. Dual, *Adv. Funct. Mater.* **2009**, *19*, 1215.
- [50] J. Holz, F. K. Schulte, H. Wagner, *Solid Surface Physics*, Springer, Berlin **1979**.

- [51] J. L. Aragonés, L. G. MacDowell, C. Vega, *J. Phys. Chem. A* **2011**, *115*, 5745.
- [52] G. Greczynski, T. Kugler, W. R. Salaneck, *Thin Solid Films* **1999**, *354*, 129.
- [53] A. Lenz, H. Kariis, A. Pohl, P. Persson, L. Ojamäe, *Chem. Phys.* **2011**, *384*, 44.
- [54] A. M. Nardes, M. Kemerink, R. A. J. Janssen, *Phys. Rev. B* **2007**, *76*, 085208.
- [55] T. Horii, Y. Li, Y. Mori, H. Okuzaki, *Polym. J.* **2015**, *47*, 695.
- [56] N. Koch, A. Vollmer, *Appl. Phys. Lett.* **2006**, *89*, 162107.
- [57] J.-P. Yang, L.-T. Shang, F. Bussolotti, L.-W. Cheng, W.-Q. Wang, X.-H. Zeng, S. Kera, Y.-Q. Li, J.-X. Tang, N. Ueno, *Org. Electron.* **2017**, *48*, 172.